

Controllable Coupled Image Generation via Diffusion Models

Chenfei Yuan* Nanshan Jia*† Hangqi Li* Peter W. Glynn Zeyu Zheng

Abstract

We provide an attention-level control method for the task of coupled image generation, where “coupled” means that multiple simultaneously generated images are expected to have the same or very similar backgrounds. While backgrounds coupled, the centered objects in the generated images are still expected to enjoy the flexibility raised from different text prompts. The proposed method disentangles the background and entity components in the model’s cross-attention modules, attached with a sequence of time-varying weight control parameters depending on the time step of sampling. We optimize this sequence of weight control parameters with a combined objective that assesses how coupled the backgrounds are as well as text-to-image alignment and overall visual quality. Empirical results demonstrate that our method outperforms existing approaches across these criteria.

1 Introduction

Diffusion models, since Ho et al. [2020], Song et al. [2020a,b], Lipman et al. [2022], have emerged as a powerful tool for generative modeling, achieving remarkable success in generating high-quality images and videos given textual prompts. By iteratively denoising random noise guided by learned data distributions, these models have surpassed prior generative models, such as GAN Goodfellow et al. [2014, 2020] and variational autoencoders Kingma et al. [2013], in both sample quality and diversity Dhariwal and Nichol [2021]. Their ability to synthesize diverse and realistic visual content has led to rapid adoption in a wide range of creative and industrial applications, including digital art, animation, design, and content creation Rombach et al. [2022], Saharia et al. [2022].

On top of these advancements, researchers and practitioners have expressed growing desires and interests in more-controllable generation Epstein et al. [2023], Qin et al. [2023], Gaintseva et al. [2025]. More-controllable generation refers to the ability to influence and constrain specific aspects of the generated output, such as maintaining very similar backgrounds Hertz et al. [2022], ensuring precise object placement Tewel et al. [2024], Liu et al. [2024b], Ma et al. [2024], or independently modulating style and content Wu et al. [2023], Wang et al. [2023], Qi et al. [2024], Jiang and Chen [2024], Tarrés et al. [2024]. This type of fine-grained control, if manageably achieved, can be desirable for certain applications with demand for consistency, reliability, and interpretability, such as media synthesis, image editing, and design automation Zhang et al. [2023b,a], Mou et al. [2024].

In this work, we study an image generation task called coupled image generation, which aims to achieve more controllability in terms of simultaneously generating multiple images with the same or highly similar backgrounds. The input consists of prompts that describe similar backgrounds but differ in the main objects, which we referred to as the entities. This difference may arise from entirely different entities, or from the same entity presented with variations in angle, position, or appearance. While the backgrounds across generated images are expected to be coupled and controlled, the entities are expected to vary according to the prompt-specific description. Below we present an example of the coupled image generation task.

*Chenfei Yuan, Nanshan Jia and Hangqi Li contributed equally to this work.

†Corresponding author. UC Berkeley IEOR and BAIR. nsjia@berkeley.edu

Baseline method (Flux) for coupled image generation



(a) Prompt: A cute Pikachu sits on the floor of a cozy room bathed in warm sunshine. The room has wooden flooring and a peaceful, homely atmosphere.



(b) Prompt: A cute Pikachu **stands** on the floor of a cozy room bathed in warm sunshine. The room has wooden flooring and a peaceful, homely atmosphere.



(c) Prompt: A **beautiful girl** stands on the floor of a cozy room bathed in warm sunshine. The room has wooden flooring and a peaceful, homely atmosphere.

Our method for coupled image generation



(d) Prompt: A cute Pikachu sits on the floor of a cozy room bathed in warm sunshine. The room has wooden flooring and a peaceful, homely atmosphere.



(e) Prompt: A cute Pikachu **stands** on the floor of a cozy room bathed in warm sunshine. The room has wooden flooring and a peaceful, homely atmosphere.



(f) Prompt: A **beautiful girl** stands on the floor of a cozy room bathed in warm sunshine. The room has wooden flooring and a peaceful, homely atmosphere.

Figure 1: The first row illustrates that by given prompts that have almost the same description and differ only slightly in the subject, the pictures generated by Flux Labs [2024a] have significant background differences, even after using the same random seeds in every step and using the same sampling settings. The second row illustrates the coupled generated images using our method, where the generated images share very similar backgrounds.

Coupled image generation has several practical applications. For example, some video generation models take the first and last frames as input to generate intermediate frames while ensuring temporal coherence Kuaishou Technology [2024], Jain et al. [2024], Liu et al. [2024a], Alibaba Tongyi Wanxiang Team [2025]. In such cases, maintaining a highly similar background across these frames is essential for temporal consistency among frames. Coupled image generation also benefit 3D modeling, particularly in multi-view reconstruction tasks. As noted in Hu et al. [2020], Caliskan et al. [2020], accurate 3D reconstruction typically necessitates multiple views of an object captured from different angles. Ensuring a consistent and similar background across these views contribute to isolating the object’s shape and enhancing stability during the modeling process. Additionally, coupled image generation can support image editing tasks. Certain editing applications require modifying only the foreground while preserving the background. For example, Li et al. [2023a] proposes methods that modify the primary object while keeping the rest of the scene features consistent. These tasks typically rely on datasets consisting of paired images with similar backgrounds and varying foreground entities. Coupled image generation offers an efficient tool to construct such datasets.

Prior to our work, several methods have been proposed that directly or indirectly address the coupled image generation task. These approaches can be broadly classified into three categories: image composition, image editing, and attention control. Image composition methods Ye et al. [2023], Creative [2024] typically begin with a given image depicting the background and then insert an entity based on the input prompt. The insertion step either adopts inpainting-based techniques or employs models specifically designed for direct object addition. These methods require additional input on the background image and often struggle with maintaining global consistency, such as lighting, shadows, and texture, resulting in visual artifacts. Image editing techniques for coupled image generation Rout et al. [2024], Black Forest Labs [2025] typically generate images separately. In practice, these methods often begin by generating an image based on one of the prompts and then editing it to align with the descriptions provided by other prompts. While such methods allow for localized control, they often require substantial manual input and tend to generalize not well across diverse prompts or complex scenes. Moreover, these methods are computationally less efficient, as each image must be generated individually. Finally, attention editing methods Hertz et al. [2022], Yang et al. [2023], Wang et al. [2024b], Chen et al. [2024] conduct image generation by manipulating the cross-attention maps within diffusion models to emphasize specific content. Techniques such as prompt-to-prompt editing Hertz et al. [2022] and token-level attention injection Wang et al. [2024b] enable partial control over shared backgrounds by implicitly disentangling background and foreground descriptions. However, these methods are often sensitive to prompt formulation and may struggle to preserve spatial or semantic consistency when applied across multiple generations. We leave a more thorough discussion on related literature in the supplementary materials.

To address the limitations of existing methods, we propose a cross-attention control framework for coupled image generation. Our approach introduces a combined evaluation metric that jointly measures background similarity and text-to-image alignment for generated images. Inspired by prior work on attention editing, we first employ a pre-trained large language model (LLM) to explicitly disentangle the input prompts. The LLM is prompted to extract a shared background prompt and an entity prompt from each input. This decomposition enables separate control over the background and entity during generation. We then modify the cross-attention module in the diffusion model to accept two text sources. Specifically, we introduce an auxiliary parameter that controls the relative influence of the background and entity prompts within the cross-attention mechanism. To optimize this parameter, we formulate an isotonic optimization problem guided by the proposed evaluation metric. Empirically, we show that our method achieves both high background similarity and strong text-image alignment with minimal additional training. We summarize our contributions as follows:

1. We formalize the task of coupled image generation, where multiple prompts share a very similar background while differing in foreground entities. To evaluate performance on this task, we propose an evaluation metric that jointly captures background similarity and text-image alignment.
2. After explicitly disentangling each prompt into a background and an entity component, we adapt the model’s cross-attention layers to handle them jointly and integrate a sequence of time-varying tunable parameters controlling their relative weights.
3. We frame the learning of this sequence of parameters as an isotonic optimization problem, which allows for efficient and stable training. Experiments across standard benchmarks

show improvements in both background similarity and alignment with entity prompts. Such improvements are achieved without losing inference and sampling efficiency.

2 Background on Cross-attention Mechanism

Cross-attention is an attention mechanism that allows one sequence to attend to another sequence. Instead of computing attention within a single sequence like self-attention, cross-attention aligns the information from one sequence to another through the calculation of attention. This enables the model to dynamically focus on the most relevant parts of the input when generating or interpreting output. The concept was first introduced by Bahdanau et al. [2014] in the context of neural machine translation, where a decoder RNN is set to align with the encoder hidden states. Since then, cross-attention has become a core architectural component in text-to-image generation. In this setting, it enables alignment between visual features and the input text, allowing the model to condition each generated visual element on specific words or phrases from the prompt. This ensures that the output image accurately and coherently reflects the described content.

In what follows, we briefly introduce two types of cross-attention mechanisms commonly used in text-to-image generation models.

1. **QKV-level concatenation-based cross-attention.** This cross-attention mechanism first computes the (query, key, value) tuple for both text embeddings and image hidden state. Then, queries, keys and values are concatenated before sending to the attention mechanism. The mathematical formulation is given by

$$\text{Attention}(Q_{\text{joint}}, K_{\text{joint}}, V_{\text{joint}}) = \text{softmax} \left(\frac{Q_{\text{joint}} K_{\text{joint}}^\top}{\sqrt{d_{\text{text}} + d_{\text{img}}}} \right) V_{\text{joint}}, \quad (1)$$

where $Q_{\text{joint}} = [Q_{\text{text}}, Q_{\text{img}}]$, $K_{\text{joint}} = [K_{\text{text}}, K_{\text{img}}]$, $V_{\text{joint}} = [V_{\text{text}}, V_{\text{img}}]$, d_{text} is the hidden dimension of textual prompts and d_{img} is the hidden dimension of image hidden state. Following the cross-attention module, the outputs are split into text and image components, each of which is independently processed by subsequent projection layers.

2. **Embedding-level concatenation-based cross-attention.** Embeddings from different modalities are first concatenated into a unified sequence. Then, a standard self-attention is applied uniformly across this sequence. Although the concatenated sequence is used for self-attention, the method acts as cross-attention because attention weights can form between tokens from different modalities. This allows each modality to attend to the other. Specifically, define $X_{\text{concat}} = [X_{\text{text}}; X_{\text{img}}]$ and calculate corresponding query, key and value, where subscript "concat" are added. The attention comes as

$$\text{Attention}(Q_{\text{concat}}, K_{\text{concat}}, V_{\text{concat}}) = \text{softmax} \left(\frac{Q_{\text{concat}} K_{\text{concat}}^\top}{\sqrt{d_{\text{concat}}}} \right) V_{\text{concat}}, \quad (2)$$

where d_{concat} is the hidden dimension of the concatenated embedding X_{concat} . The attention output from the cross-attention module is further processed by subsequent layers, ultimately producing the output of the block.

For each type of cross-attention, we will introduce our cross-attention control method in Section 4.2.

3 Problem Formulation

We now formalize the coupled image generation problem. The term "coupled" refers to generating multiple images simultaneously that share the same or very similar backgrounds while differing in their depicted entities, based on input prompts. Suppose that we have a pre-trained text-to-image generation model $G : \mathbb{T} \rightarrow \mathbb{I}$, where \mathbb{T} is the prompt space and \mathbb{I} is the space of generated images, we parameterize it with an auxiliary vector $\theta \in \Theta$ and denote it by G_θ . The detailed parameterization method is included in Section 4.2 later. Then, given a batch size n and input prompts $T_1, T_2, \dots, T_n \in \mathbb{T}$, we feed these inputs to G_θ and denote the generated images by $I_j = G_\theta(T_j)$ for $j = 1, 2, \dots, n$.

To evaluate whether the generated images meet the requirements of coupled image generation problem, we define the following objectives:

1. **Background similarity.** A function $f_{bg} : \mathbb{T}^n \times \mathbb{I}^n \rightarrow \mathbb{R}^+$ that measures the degree of background similarity across the generated samples. Higher values indicate stronger background similarity across the function inputs.
2. **Text-image alignment.** A function $f_{ti} : \mathbb{T} \times \mathbb{I} \rightarrow \mathbb{R}^+$, where $f_{ti}(T, I)$ quantifies how well image I aligns with prompt T . Higher values indicate stronger alignment between the image and the prompt.

Given weight parameters $\lambda_{bg}, \lambda_{ti}$, we define the combined objective $f_c : \mathbb{T}^n \times \Theta \rightarrow \mathbb{R}^+$ as

$$f_c(T_1, \dots, T_n, \theta) = \lambda_{bg} f_{bg}(T_1, \dots, T_n, G_\theta(T_1), \dots, G_\theta(T_n)) + \frac{\lambda_{ti}}{n} \sum_{j=1}^n f_{ti}(T_j, G_\theta(T_j)). \quad (3)$$

The training of θ is then formulated as solving the optimization problem:

$$\max_{\theta \in \Theta} \frac{1}{M} \sum_{k=1}^M f_c(T_{k,1}, \dots, T_{k,n}, \theta), \quad (4)$$

where $\{T_{k,1}, \dots, T_{k,n}\}$ denotes the k -th training set.

4 Our Method

As shown in Section 1 and Figure 1, the backgrounds of images generated by the pre-trained model G exhibit noticeable visual differences, even when the prompts describe the same or highly similar background and the random seed is manually fixed. We attribute this phenomenon to the lack of explicit disentanglement between background and entity in most text-to-image generation models, such as Flux Labs [2024b] and Stable Diffusion Rombach et al. [2022]. The presence of different entities in the prompt can affect spatial layout, lighting and texture through the cross-attention modules during each denoising step. With accumulation occurring across all steps during inference, this affection eventually results in variations and differences in the background of the generated images and the overall image composition.

To overcome this entanglement in prompt, we first propose a disentanglement method in Section 4.1, which extracts the shared background information from all prompts and presents entity prompt for each individual prompt. Then, we introduce our method to incorporate both background prompt and entity prompt in Section 4.2. We finally formalize the isotonic optimization problem in Section 4.3.

4.1 Explicitly Disentangling Prompts into Background Prompts and Entity Prompts

Our method begins by reorganizing the input prompts to disentangle shared and distinct components. Specifically, given input prompts $T_1, \dots, T_n \in \mathbb{T}$, we use a pre-trained large language model to extract a shared background prompt and distinct entity prompts. The model outputs a background prompt T_{bg} and a set of entity prompts $T_1^{\text{ent}}, \dots, T_n^{\text{ent}}$. The background prompt captures the shared background information across all inputs and each entity prompt describes the unique entity in its corresponding input. A concrete example of this decomposition process is illustrated in Figure 2.

4.2 Cross-attention Control

Most cross-attention modules in text-to-image generation models only takes one text embedding and one image hidden state as input. Given our scope of coupled image generation, after the prompt being disentangled into background prompt and entity prompt, we modify the cross-attention module to enable two input text embeddings. In addition, as outlined in Section 3, we want the generated images to share a very similar background with high alignment between prompt and image. Hence, we have to control the relative weight of background prompt and entity prompt. To this end, we introduce our cross-attention control method for different types of cross-attention as follows. For ease of exposition, we will use subscript bg , ent and img to denote background, entity and image, respectively.

1. **QKV-level concatenation-based cross-attention.** To extend the QKV-level concatenation-based cross-attention mechanism, we propose to concatenate the query, key, and value

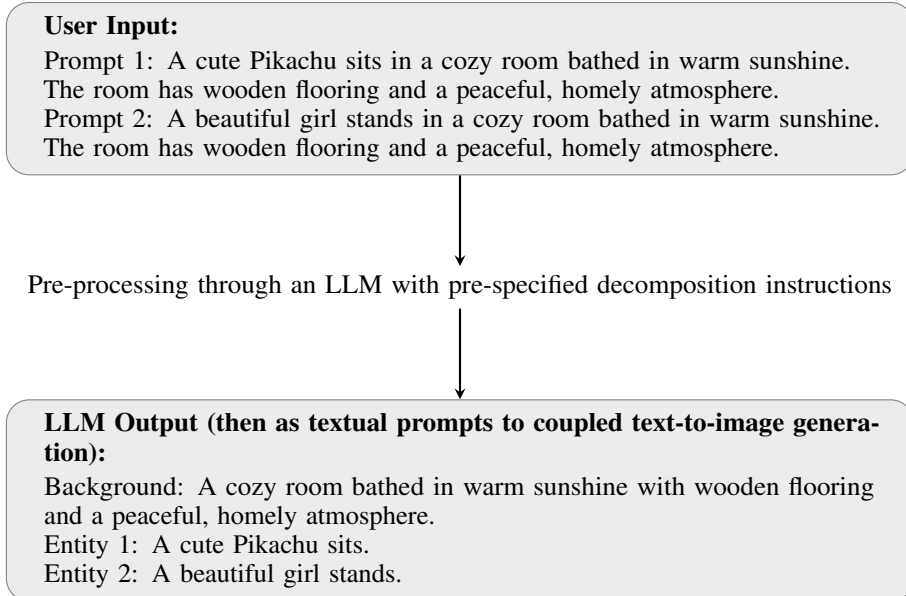


Figure 2: A zero-shot example of prompting a pre-trained LLM to extract the shared background from a set of prompts and present the distinct entity descriptions for each individual prompt. The pre-specified prompt for LLM can be found in the supplementary materials.

vectors across the background embedding, entity embedding, and image hidden states. Specifically, we define

$$\text{Attention}(Q_{\text{joint}}, K_{\text{joint}}(\theta), V_{\text{joint}}) = \text{softmax} \left(\frac{Q_{\text{joint}} K_{\text{joint}}^{\top}(\theta)}{\sqrt{d_{\text{text}} + d_{\text{img}}}} \right) V_{\text{joint}}, \quad (5)$$

where $\theta \in [0, 1]$, $Q_{\text{joint}} = [Q_{\text{bg}}, Q_{\text{ent}}, Q_{\text{img}}]$, $K_{\text{joint}}(\theta) = [(1-\theta)K_{\text{bg}}, \theta K_{\text{ent}}, K_{\text{img}}]$, and $V_{\text{joint}} = [V_{\text{bg}}, V_{\text{ent}}, V_{\text{img}}]$.

Next, we elaborate on the parameterization in (5). There are two key design choices. First, we scale the key vectors by $(1-\theta)$ for the background and by θ for the entity. The auxiliary parameter θ serves as a soft weighting factor between the background and the entity. When θ is close to 1, the entity contributes more prominently to the attention scores. Conversely, when θ is close to 0, the background dominates.

Second, although the concatenated query, key, and value vectors have total dimension $2d_{\text{text}} + d_{\text{img}}$, we normalize the dot product in the softmax using $\sqrt{d_{\text{text}} + d_{\text{img}}}$ instead of $\sqrt{2d_{\text{text}} + d_{\text{img}}}$. This choice of normalization by $\sqrt{d_{\text{text}} + d_{\text{img}}}$ comes from the fact that only the background and entity contribute to the modulated key vectors in the attention score. Since the image component remains unscaled, using $\sqrt{d_{\text{text}} + d_{\text{img}}}$ instead of $\sqrt{2d_{\text{text}} + d_{\text{img}}}$ ensures that the overall scale of the attention scores remains consistent with the original case (1). In addition, this normalization ensures that, when $\theta = 1$, the attention weights are reduced exactly to the original cross-attention weights (1) using only the entity embedding, and, when $\theta = 0$, they are reduced to the cross-attention weights that only use the background embedding. Together, these two design choices allow our parameterization to provide fine-grained control over attention composition while preserving semantic consistency in the output.

- 2. Embedding-level concatenation-based cross-attention.** In the embedding-level concatenation-based cross-attention, directly concatenating the background and entity embeddings with the image hidden state would alter the architecture, as the multi-layer perceptron following the cross-attention module is designed to accept inputs of dimension $2d$. To avoid the need for auxiliary training or architectural adjustments in each block, we propose a method that accommodates both background and entity embeddings while preserving the original architecture. We first perform embedding-level concatenation:

$$X_{\text{bg-img}} = [X_{\text{bg}}; X_{\text{img}}], \quad X_{\text{ent-img}} = [X_{\text{ent}}; X_{\text{img}}], \quad (6)$$

where X_{img} is the image hidden state, and $X_{\text{bg}}, X_{\text{ent}}$ are the background and entity embeddings, respectively. We then compute the cross-attention separately for each concatenated input:

$$\text{Attention}(Q_{\text{bg-img}}, K_{\text{bg-img}}, V_{\text{bg-img}}) = \text{softmax} \left(\frac{Q_{\text{bg-img}} K_{\text{bg-img}}^\top}{\sqrt{d_{\text{concat}}}} \right) V_{\text{bg-img}}, \quad (7)$$

$$\text{Attention}(Q_{\text{ent-img}}, K_{\text{ent-img}}, V_{\text{ent-img}}) = \text{softmax} \left(\frac{Q_{\text{ent-img}} K_{\text{ent-img}}^\top}{\sqrt{d_{\text{concat}}}} \right) V_{\text{ent-img}}. \quad (8)$$

After the cross-attention operation, the background-image and entity-image attention outputs are propagated separately through subsequent layers. Let the outputs be denoted as:

$$X'_{\text{bg-img}} = [X'_{\text{bg}}; X_{\text{img-bg}}], \quad X'_{\text{ent-img}} = [X'_{\text{ent}}; X_{\text{img-ent}}]. \quad (9)$$

We then merge the image hidden states by weighted interpolation:

$$X'_{\text{img}} = \theta X_{\text{img-ent}} + (1 - \theta) X_{\text{img-bg}}, \quad (10)$$

and redefine the block outputs as

$$X'_{\text{bg-img}} = [X'_{\text{bg}}; X'_{\text{img}}], \quad X'_{\text{ent-img}} = [X'_{\text{ent}}; X'_{\text{img}}]. \quad (11)$$

This formulation ensures that the image hidden state remains unified and consistent across both branches after each block. Each block output serves as the input to the subsequent block.

We also note that, although the introduction of θ occurs after the cross-attention module, the method still enjoys the following property: when $\theta = 1$, the entity-image branch reduces exactly to the original block output that uses only the entity embedding; and when $\theta = 0$, the background-image branch reduces to the output of the original cross-attention block that uses only the background embedding. This design ensures compatibility with existing architectures while enabling interpolation between background embedding and entity embedding in shaping and guiding the image hidden states.

4.3 Formulation of an Isotonic Problem to Optimize a Parameterized Model

Given a pre-trained text-to-image generation model G , we first introduce our parameterization method. Assume a given time schedule that supports an N -step inference. We propose a parameterized model G_θ , where $\theta \in \Theta$, such that each cross-attention module at the i -th inference step is parameterized by θ_i , following the approach detailed in Section 4.2. Inspired by previous findings Choi et al. [2022], Park et al. [2023], Yue et al. [2024], Wang et al. [2024a] that diffusion models initially focus on generating coarse structure and subsequently refining fine-grained details, we impose an ascending order constraint on the parameter sequence $\{\theta_i\}$ to align with this progressive refinement process and stabilize the training. That said, we formulate the problem of learning θ as an isotonic optimization problem:

$$\begin{aligned} \max_{\theta} & \frac{1}{M} \sum_{k=1}^M f_c(T_{k,1}, \dots, T_{k,n}, \theta), \\ \text{subject to} & \theta_1 \leq \theta_2 \leq \dots \leq \theta_N, \\ & \theta \in \Theta. \end{aligned} \quad (12)$$

In the constraints, we impose an ascending order on the parameter sequence $\{\theta_i\}$. This ordering reflects the growing influence of entity-specific information over time, alongside the diminishing effect of background information. It reveals how the model gradually shifts its attention from shared background features in the early inference steps to entity-specific details in the later steps. This progressive shift ensures that the generated images share a consistent background while achieving high text-image alignment through the later incorporation of entity prompts.

5 Experiments

5.1 Experimental Settings

5.1.1 Base Text-to-Image Generation Model

Throughout the paper, we use Flux.1dev Labs [2024a] as the base model G . In the Flux architecture, there are 19 double-stream blocks and 38 single-stream blocks. Each double-stream block employs QKV-level concatenation-based cross-attention, followed by independent feedforward layers and layer normalization for the text embedding and image hidden states separately. After the double-stream blocks, the text embedding is concatenated with the image hidden states and passed to the single-stream blocks. These blocks use embedding-level concatenation-based cross-attention, followed by a unified feedforward network and layer normalization. We consider generating images with resolution 1024×1024 with 50 steps. Guidance scale is set to be 3.5. In this case, the time-varying parameter θ is a 50-dimensional vector under the isotomic constraint

$$0 \leq \theta_1 \leq \theta_2 \leq \dots \leq \theta_{50} \leq 1$$

. At the i -th step, all cross-attention modules are parameterized with θ_i following the cross-attention control method introduced in Section 4.2. All experiments are conducted on a single NVIDIA A100 GPU.

5.1.2 Implementation Details on Proposed Metrics.

We have proposed a combined metric to evaluate both background similarity and text-image alignment in Section 3. In this section, we introduce our implementation of the functions f_{bg} and f_{ti} . We begin with f_{bg} . For each prompt T_j , we follow the proposed method to generate the corresponding image I_j . We then use the Segment Anything model Kirillov et al. [2023] to segment the foreground entity. Specifically, let A_j denote the region in image I_j that is segmented as the entity. We define the Joint Entity Region (JER) as

$$\text{JER} = A_1 \cup A_2 \cup \dots \cup A_n. \quad (13)$$

For each image, we apply the same mask over the JER. We then compute the average \mathbb{L}^2 distance between the masked images. To account for the proportion of unmasked regions, we define a validity ratio:

$$R = 1 - \frac{\#\text{JER}}{\text{width} \times \text{height}}, \quad (14)$$

where $\#\text{JER}$ denotes the number of pixels contained in the JER, and width, height refer to the resolution of the generated images.

We scale the average \mathbb{L}^2 distance by this ratio and define the background similarity function as

$$f_{bg} = -\frac{2}{n(n-1)R} \sum_{1 \leq j < k \leq n} \|\text{mask} \circ I_j - \text{mask} \circ I_k\|^2, \quad (15)$$

where $\text{mask} \circ$ denotes the masking operation on the JER, and $\|\cdot\|$ denotes the \mathbb{L}^2 norm.

For f_{ti} , we adopt the CLIPScore Radford et al. [2021], Hessel et al. [2021]. CLIPScore is a reference-free evaluation metric for text-to-image generation that uses the CLIP model’s cross-modal embedding space. It operates by encoding both the image and the associated textual prompt into a shared semantic space using CLIP’s pre-trained encoders. The metric then computes the cosine similarity between these two embeddings to quantify the degree to which the image content aligns with the textual description. A higher CLIPScore typically indicates better text-image alignment. In the following experiments, we always choose $\lambda_{bg} = 300$ and $\lambda_{ti} = \frac{1}{30}$ for proper normalization.

5.2 Comparison to Other Methods

In this section, we compare our method with existing approaches for the coupled image generation task. We consider the following baselines:

1. **Random seed.** This baseline generates images using the Flux model with a fixed random seed to encourage consistency across outputs.

2. **P2P.** The Prompt-to-Prompt method Hertz et al. [2022] edits the cross-attention maps within the Flux model to enforce alignment between similar prompts.
3. **RF-inversion.** The RF-inversion method Rout et al. [2024] first generates an image from a given prompt and then applies an inversion-based editing process to align it with other prompts.

We present the generated images in Figure 3. The prompts used are: "An eagle soars gracefully in a vibrant meadow under a clear blue sky, bathed in sunlight." and "A red fox runs in a vibrant meadow under a clear blue sky, bathed in sunlight.". We observe that both our method and P2P produce images with highly similar backgrounds. In contrast, editing-based methods, such as RF-inversion, fail to ensure strong background similarity. Moreover, our method outperforms P2P in terms of text-image alignment, as it more accurately and clearly depicts the specified entities. Overall, our method yields the highest combined metric. Additionally, we report the evaluation metrics for all methods in Table 1. These data supports our visual observations.

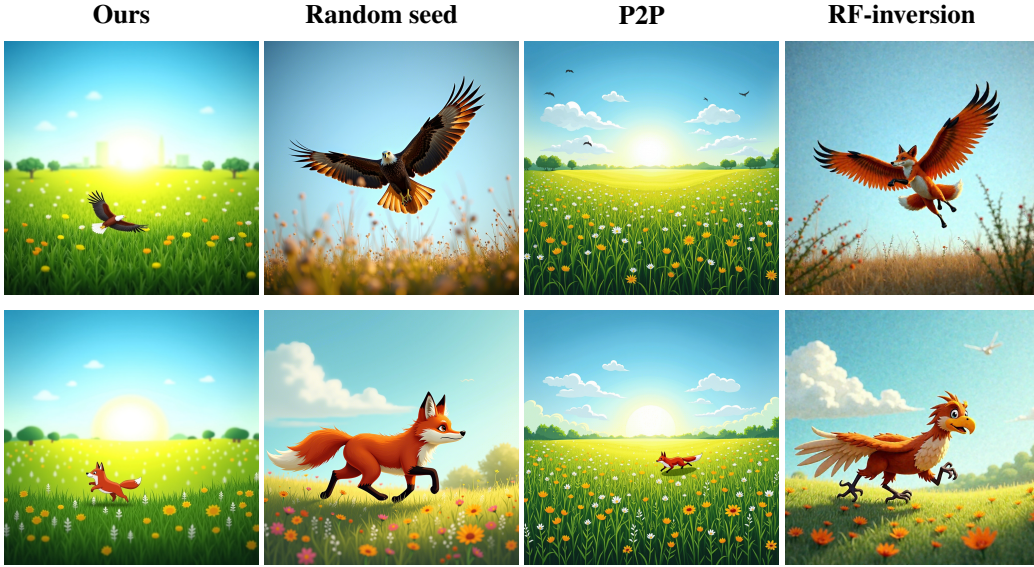


Figure 3: Comparison of our method to other baselines. Generated pictures in the first row correspond to prompt: "An eagle soars gracefully in a vibrant meadow under a clear blue sky, bathed in sunlight.". The second row corresponds to prompt: "A red fox runs in a vibrant meadow under a clear blue sky, bathed in sunlight." Our method performs better than baselines in both background similarity and text-image alignment, where our method and all baseline methods share the same sampling procedures and random numbers.

Table 1: Metrics for coupled image generation

Metrics \Model.	Ours	Random seed	P2P	RF-inversion
Background similarity ($\times 10^{-4}$) (\uparrow)	-2.080	-67.42	-4.604	-48.47
Text-image alignment (\uparrow)	22.61	18.75	18.14	19.59
Combined metric (\uparrow)	1.558	-0.919	1.246	-0.214

6 Conclusion and Future Work

In this work, we formalize the coupled image generation task, which aims to generate multiple images simultaneously while preserving a highly similar background. We propose a combined metric that jointly measures background similarity and text-image alignment. This metric can be used to evaluate the performance on coupled image generation task. To achieve coupled generation, we first explicitly disentangle each input prompt into a shared background prompt and individual entity prompts. We

then introduce a cross-attention control mechanism that enables the model to process and balance these disentangled components. A sequence of time-varying parameters is introduced to control the relative influence of background and entity prompts across the inference steps. We formulate the learning of these parameters as an isotonic optimization problem to enhance training stability and efficiency. Through extensive comparisons with prior methods, we demonstrate that our approach improves both background similarity and text-image fidelity. Notably, our method does not sacrifice inference or sampling efficiency.

We would love to point out a few limitations of our work. First, our work only handles text-to-image generation and does not consider the task of image generations with multi-modal inputs. Second, the approach introduces time-varying parameters on cross-attention mechanisms, which may introduce scalability issues when generating complex scenes or long sequences (e.g., video frames), where balancing multiple components becomes more challenging.

References

- Alibaba Tongyi Wanxiang Team. Wan 2.1 flf2v: First-last frame video generation. <https://www.runcomfy.com/comfyui-workflows/wan-2-1-flf2v-first-last-frame-video-generation>, 2025. Accessed: May 14, 2025.
- Omri Avrahami, Dani Lischinski, and Ohad Fried. Blended diffusion for text-driven editing of natural images. In *Proceedings of the IEEE/CVF conference on computer vision and pattern recognition*, pages 18208–18218, 2022.
- Dzmitry Bahdanau, Kyunghyun Cho, and Yoshua Bengio. Neural machine translation by jointly learning to align and translate. *arXiv preprint arXiv:1409.0473*, 2014.
- Black Forest Labs. Flux.1 redux [dev]: Image variation adapter for flux.1 models. <https://huggingface.co/black-forest-labs/FLUX.1-Redux-dev>, 2025.
- Tim Brooks, Aleksander Holynski, and Alexei A Efros. Instructpix2pix: Learning to follow image editing instructions. In *Proceedings of the IEEE/CVF conference on computer vision and pattern recognition*, pages 18392–18402, 2023.
- Akin Caliskan, Armin Mustafa, Evren Imre, and Adrian Hilton. Multi-view consistency loss for improved single-image 3d reconstruction of clothed people. In *Proceedings of the Asian Conference on Computer Vision*, 2020.
- Mingdeng Cao, Xintao Wang, Zhongang Qi, Ying Shan, Xiaohu Qie, and Yinqiang Zheng. Masactrl: Tuning-free mutual self-attention control for consistent image synthesis and editing. In *Proceedings of the IEEE/CVF international conference on computer vision*, pages 22560–22570, 2023.
- Minghao Chen, Iro Laina, and Andrea Vedaldi. Training-free layout control with cross-attention guidance. In *Proceedings of the IEEE/CVF winter conference on applications of computer vision*, pages 5343–5353, 2024.
- Jooyoung Choi, Jungbeom Lee, Chaehun Shin, Sungwon Kim, Hyunwoo Kim, and Sungroh Yoon. Perception prioritized training of diffusion models. In *Proceedings of the IEEE/CVF Conference on Computer Vision and Pattern Recognition*, pages 11472–11481, 2022.
- Alimama Creative. Flux.1-dev-controlnet-inpainting-beta. <https://huggingface.co/alimama-creative/FLUX.1-dev-Controlnet-Inpainting-Beta>, 2024.
- Prafulla Dhariwal and Alexander Nichol. Diffusion models beat gans on image synthesis. *Advances in neural information processing systems*, 34:8780–8794, 2021.
- Xiaoyi Dong, Pan Zhang, Yuhang Zang, Yuhang Cao, Bin Wang, Linke Ouyang, Xilin Wei, Songyang Zhang, Haodong Duan, Maosong Cao, et al. Internlm-xcomposer2: Mastering free-form text-image composition and comprehension in vision-language large model. *arXiv preprint arXiv:2401.16420*, 2024.

- Dave Epstein, Allan Jabri, Ben Poole, Alexei A. Efros, and Aleksander Holynski. Diffusion self-guidance for controllable image generation. 2023.
- Tatiana Gaintseva, Chengcheng Ma, Ziquan Liu, Martin Benning, Gregory Slabaugh, Jiankang Deng, and Ismail Elezi. Casteer: Steering diffusion models for controllable generation. *arXiv preprint arXiv:2503.09630*, 2025.
- Ian Goodfellow, Jean Pouget-Abadie, Mehdi Mirza, Bing Xu, David Warde-Farley, Sherjil Ozair, Aaron Courville, and Yoshua Bengio. Generative adversarial networks. *Communications of the ACM*, 63(11):139–144, 2020.
- Ian J Goodfellow, Jean Pouget-Abadie, Mehdi Mirza, Bing Xu, David Warde-Farley, Sherjil Ozair, Aaron Courville, and Yoshua Bengio. Generative adversarial nets. *Advances in neural information processing systems*, 27, 2014.
- Amir Hertz, Ron Mokady, Jay Tenenbaum, Kfir Aberman, Yael Pritch, and Daniel Cohen-Or. Prompt-to-prompt image editing with cross attention control. *arXiv preprint arXiv:2208.01626*, 2022.
- Jack Hessel, Ari Holtzman, Maxwell Forbes, Ronan Le Bras, and Yejin Choi. Clipscore: A reference-free evaluation metric for image captioning. *arXiv preprint arXiv:2104.08718*, 2021.
- Jonathan Ho, Ajay Jain, and Pieter Abbeel. Denoising diffusion probabilistic models. *Advances in neural information processing systems*, 33:6840–6851, 2020.
- Tao Hu, Zhizhong Han, and Matthias Zwicker. 3d shape completion with multi-view consistent inference. In *Proceedings of the AAAI conference on artificial intelligence*, volume 34, pages 10997–11004, 2020.
- Satoshi Iizuka, Edgar Simo-Serra, and Hiroshi Ishikawa. Globally and locally consistent image completion. *ACM Transactions on Graphics (ToG)*, 36(4):1–14, 2017.
- Siddhant Jain, Daniel Watson, Eric Tabellion, Ben Poole, Janne Kontkanen, et al. Video interpolation with diffusion models. In *Proceedings of the IEEE/CVF Conference on Computer Vision and Pattern Recognition*, pages 7341–7351, 2024.
- Ruixiang Jiang and Changwen Chen. Artist: Aesthetically controllable text-driven stylization without training. *arXiv preprint arXiv:2407.15842*, 2024.
- Bahjat Kawar, Shiran Zada, Oran Lang, Omer Tov, Huiwen Chang, Tali Dekel, Inbar Mosseri, and Michal Irani. Imagic: Text-based real image editing with diffusion models. In *Proceedings of the IEEE/CVF conference on computer vision and pattern recognition*, pages 6007–6017, 2023.
- Yunji Kim, Jiyoung Lee, Jin-Hwa Kim, Jung-Woo Ha, and Jun-Yan Zhu. Dense text-to-image generation with attention modulation. In *Proceedings of the IEEE/CVF International Conference on Computer Vision*, pages 7701–7711, 2023.
- Diederik P Kingma, Max Welling, et al. Auto-encoding variational bayes, 2013.
- Alexander Kirillov, Eric Mintun, Nikhila Ravi, Hanzi Mao, Chloe Rolland, Laura Gustafson, Tete Xiao, Spencer Whitehead, Alexander C Berg, Wan-Yen Lo, et al. Segment anything. In *Proceedings of the IEEE/CVF international conference on computer vision*, pages 4015–4026, 2023.
- Rolf Köhler, Christian Schuler, Bernhard Schölkopf, and Stefan Harmeling. Mask-specific inpainting with deep neural networks. In *Pattern Recognition: 36th German Conference, GCPR 2014, Münster, Germany, September 2-5, 2014, Proceedings 36*, pages 523–534. Springer, 2014.
- Kuaishou Technology. Kuaishou unveils proprietary video generation model 'kling'. <https://ir.kuaishou.com/news-releases/news-release-details/kuaishou-unveils-proprietary-video-generation-model-kling>, 2024. Accessed: May 14, 2025.
- Black Forest Labs. Flux.1 [dev]. <https://huggingface.co/black-forest-labs/FLUX.1-dev>, 2024a.
- Black Forest Labs. Flux. <https://github.com/black-forest-labs/flux>, 2024b.

- Donghoon Lee, Sifei Liu, Jinwei Gu, Ming-Yu Liu, Ming-Hsuan Yang, and Jan Kautz. Context-aware synthesis and placement of object instances. *Advances in neural information processing systems*, 31, 2018.
- Pengzhi Li, Qinxuan Huang, Yikang Ding, and Zhiheng Li. Layerdiffusion: Layered controlled image editing with diffusion models. In *SIGGRAPH Asia 2023 Technical Communications*, pages 1–4. 2023a.
- Xiang Li, Guowei Teng, Ping An, and Hai-yan Yao. Mt-gan: toward realistic image composition based on spatial features. *EURASIP Journal on Advances in Signal Processing*, 2023(1):46, 2023b.
- Yaron Lipman, Ricky TQ Chen, Heli Ben-Hamu, Maximilian Nickel, and Matt Le. Flow matching for generative modeling. *arXiv preprint arXiv:2210.02747*, 2022.
- Guilin Liu, Fitsum A Reda, Kevin J Shih, Ting-Chun Wang, Andrew Tao, and Bryan Catanzaro. Image inpainting for irregular holes using partial convolutions. In *Proceedings of the European conference on computer vision (ECCV)*, pages 85–100, 2018.
- Haozhe Liu, Shikun Liu, Zijian Zhou, Mengmeng Xu, Yanping Xie, Xiao Han, Juan C Pérez, Ding Liu, Kumara Kahatapitiya, Menglin Jia, et al. Mardini: Masked autoregressive diffusion for video generation at scale. *arXiv preprint arXiv:2410.20280*, 2024a.
- Jiacheng Liu, Hang Zhou, Shida Wei, and Rui Ma. Diffpop: Plausibility-guided object placement diffusion for image composition. In *Computer Graphics Forum*, volume 43, page e15246. Wiley Online Library, 2024b.
- Shiyu Liu, Yucheng Han, Peng Xing, Fukun Yin, Rui Wang, Wei Cheng, Jiaqi Liao, Yingming Wang, Honghao Fu, Chunrui Han, et al. Step1x-edit: A practical framework for general image editing. *arXiv preprint arXiv:2504.17761*, 2025.
- Wan-Duo Kurt Ma, Avishek Lahiri, John P Lewis, Thomas Leung, and W Bastiaan Kleijn. Directed diffusion: Direct control of object placement through attention guidance. In *Proceedings of the AAAI Conference on Artificial Intelligence*, volume 38, pages 4098–4106, 2024.
- Ron Mokady, Amir Hertz, Kfir Aberman, Yael Pritch, and Daniel Cohen-Or. Null-text inversion for editing real images using guided diffusion models. In *Proceedings of the IEEE/CVF conference on computer vision and pattern recognition*, pages 6038–6047, 2023.
- Eric N Mortensen and William A Barrett. Intelligent scissors for image composition. In *Proceedings of the 22nd annual conference on Computer graphics and interactive techniques*, pages 191–198, 1995.
- Chong Mou, Xintao Wang, Liangbin Xie, Yanze Wu, Jian Zhang, Zhongang Qi, and Ying Shan. T2i-adapter: Learning adapters to dig out more controllable ability for text-to-image diffusion models. In *Proceedings of the AAAI conference on artificial intelligence*, volume 38, pages 4296–4304, 2024.
- Yong-Hyun Park, Mingi Kwon, Jaewoong Choi, Junghyo Jo, and Youngjung Uh. Understanding the latent space of diffusion models through the lens of riemannian geometry. *Advances in Neural Information Processing Systems*, 36:24129–24142, 2023.
- Deepak Pathak, Philipp Krahenbuhl, Jeff Donahue, Trevor Darrell, and Alexei A Efros. Context encoders: Feature learning by inpainting. In *Proceedings of the IEEE conference on computer vision and pattern recognition*, pages 2536–2544, 2016.
- Quynh Phung, Songwei Ge, and Jia-Bin Huang. Grounded text-to-image synthesis with attention refocusing. In *Proceedings of the IEEE/CVF Conference on Computer Vision and Pattern Recognition*, pages 7932–7942, 2024.
- Tianhao Qi, Shancheng Fang, Yanze Wu, Hongtao Xie, Jiawei Liu, Lang Chen, Qian He, and Yongdong Zhang. Deadiff: An efficient stylization diffusion model with disentangled representations. In *Proceedings of the IEEE/CVF Conference on Computer Vision and Pattern Recognition*, pages 8693–8702, 2024.

- Can Qin, Shu Zhang, Ning Yu, Yihao Feng, Xinyi Yang, Yingbo Zhou, Huan Wang, Juan Carlos Niebles, Caiming Xiong, Silvio Savarese, et al. Unicontrol: A unified diffusion model for controllable visual generation in the wild. *arXiv preprint arXiv:2305.11147*, 2023.
- Alec Radford, Jong Wook Kim, Chris Hallacy, Aditya Ramesh, Gabriel Goh, Sandhini Agarwal, Girish Sastry, Amanda Askell, Pamela Mishkin, Jack Clark, et al. Learning transferable visual models from natural language supervision. In *International conference on machine learning*, pages 8748–8763. PmLR, 2021.
- Robin Rombach, Andreas Blattmann, Dominik Lorenz, Patrick Esser, and Björn Ommer. High-resolution image synthesis with latent diffusion models. In *Proceedings of the IEEE/CVF conference on computer vision and pattern recognition*, pages 10684–10695, 2022.
- Litu Rout, Yujia Chen, Nataniel Ruiz, Constantine Caramanis, Sanjay Shakkottai, and Wen-Sheng Chu. Semantic image inversion and editing using rectified stochastic differential equations. *arXiv preprint arXiv:2410.10792*, 2024.
- Chitwan Saharia, William Chan, Saurabh Saxena, Lala Li, Jay Whang, Emily L Denton, Kamyar Ghasemipour, Raphael Gontijo Lopes, Burcu Karagol Ayan, Tim Salimans, et al. Photorealistic text-to-image diffusion models with deep language understanding. *Advances in neural information processing systems*, 35:36479–36494, 2022.
- Jiaming Song, Chenlin Meng, and Stefano Ermon. Denoising diffusion implicit models. *arXiv preprint arXiv:2010.02502*, 2020a.
- Yang Song, Jascha Sohl-Dickstein, Diederik P Kingma, Abhishek Kumar, Stefano Ermon, and Ben Poole. Score-based generative modeling through stochastic differential equations. *arXiv preprint arXiv:2011.13456*, 2020b.
- Gemma Canet Tarrés, Dan Ruta, Tu Bui, and John Collomosse. Parasol: Parametric style control for diffusion image synthesis. In *Proceedings of the IEEE/CVF Conference on Computer Vision and Pattern Recognition*, pages 2432–2442, 2024.
- Yoad Tewel, Rinon Gal, Dvir Samuel, Yuval Atzmon, Lior Wolf, and Gal Chechik. Add-it: Training-free object insertion in images with pretrained diffusion models. *arXiv preprint arXiv:2411.07232*, 2024.
- Junyan Wang, Zhenhong Sun, Zhiyu Tan, Xuanbai Chen, Weihua Chen, Hao Li, Cheng Zhang, and Yang Song. Towards effective usage of human-centric priors in diffusion models for text-based human image generation. In *Proceedings of the IEEE/CVF Conference on Computer Vision and Pattern Recognition*, pages 8446–8455, 2024a.
- Zhizhong Wang, Lei Zhao, and Wei Xing. Stylediffusion: Controllable disentangled style transfer via diffusion models. In *Proceedings of the IEEE/CVF International Conference on Computer Vision*, pages 7677–7689, 2023.
- Zirui Wang, Zhizhou Sha, Zheng Ding, Yilin Wang, and Zhuowen Tu. Tokencompose: Text-to-image diffusion with token-level supervision. In *Proceedings of the IEEE/CVF Conference on Computer Vision and Pattern Recognition*, pages 8553–8564, 2024b.
- Qiucheng Wu, Yujian Liu, Handong Zhao, Ajinkya Kale, Trung Bui, Tong Yu, Zhe Lin, Yang Zhang, and Shiyu Chang. Uncovering the disentanglement capability in text-to-image diffusion models. In *Proceedings of the IEEE/CVF conference on computer vision and pattern recognition*, pages 1900–1910, 2023.
- Li Xu, Jimmy S Ren, Ce Liu, and Jiaya Jia. Deep convolutional neural network for image deconvolution. *Advances in neural information processing systems*, 27, 2014.
- Tao Xu, Pengchuan Zhang, Qiuyuan Huang, Han Zhang, Zhe Gan, Xiaolei Huang, and Xiaodong He. AttnGAN: Fine-grained text to image generation with attentional generative adversarial networks. In *Proceedings of the IEEE conference on computer vision and pattern recognition*, pages 1316–1324, 2018.

- Fei Yang, Shiqi Yang, Muhammad Atif Butt, Joost van de Weijer, et al. Dynamic prompt learning: Addressing cross-attention leakage for text-based image editing. *Advances in Neural Information Processing Systems*, 36:26291–26303, 2023.
- Hu Ye, Jun Zhang, Sibio Liu, Xiao Han, and Wei Yang. Ip-adapter: Text compatible image prompt adapter for text-to-image diffusion models.(2023). *arXiv preprint arXiv:2308.06721*, 2023.
- Raymond A Yeh, Chen Chen, Teck Yian Lim, Alexander G Schwing, Mark Hasegawa-Johnson, and Minh N Do. Semantic image inpainting with deep generative models. In *Proceedings of the IEEE conference on computer vision and pattern recognition*, pages 5485–5493, 2017.
- Jiahui Yu, Zhe Lin, Jimei Yang, Xiaohui Shen, Xin Lu, and Thomas S Huang. Generative image inpainting with contextual attention. In *Proceedings of the IEEE conference on computer vision and pattern recognition*, pages 5505–5514, 2018.
- Zhongqi Yue, Jiankun Wang, Qianru Sun, Lei Ji, Eric I Chang, Hanwang Zhang, et al. Exploring diffusion time-steps for unsupervised representation learning. *arXiv preprint arXiv:2401.11430*, 2024.
- Lvmin Zhang, Anyi Rao, and Maneesh Agrawala. Adding conditional control to text-to-image diffusion models. In *Proceedings of the IEEE/CVF international conference on computer vision*, pages 3836–3847, 2023a.
- Yabo Zhang, Yuxiang Wei, Dongsheng Jiang, Xiaopeng Zhang, Wangmeng Zuo, and Qi Tian. Controlvideo: Training-free controllable text-to-video generation. *arXiv preprint arXiv:2305.13077*, 2023b.

A Literature Review

Prior to our work, several methods have been proposed that, while not explicitly designed for coupled image generation, can nevertheless be adapted to this task due to their compatible input-output frameworks. These existing approaches can be broadly classified into three categories: image inpainting and composition methods, image editing methods, and attention editing methods. Image inpainting and composition methods typically require a background image as input. They then compose entities guided by textual prompts onto the background image. Image editing methods initially generate an image based on one prompt and subsequently modify this image to align with additional prompts while preserving the background context. Attention editing methods specifically target the cross-attention modules within model architectures and control background consistency through the manipulation of cross-attention maps. In the following sections, we provide a detailed literature review of each of these method categories.

A.1 Image Inpainting and Composition

Image inpainting techniques allow regenerating missing or removed regions of an image with plausible content, which can be leveraged to replace a foreground object while preserving the original background. Early deep learning approaches like Context Encoders used convolutional auto-encoders with adversarial loss to fill large missing regions Köhler et al. [2014], Xu et al. [2014], Yeh et al. [2017], Liu et al. [2018]. Follow-up works addressed limitations such as blurriness and artifacts. For example, partial convolution layers were introduced to condition only on valid pixels and ignore masked-out regions. This improves inpainting of irregular holes. Another milestone was using contextual attention to explicitly copy information from distant background patches into the hole Pathak et al. [2016], Yu et al. [2018], which greatly improved structural coherence. Subsequent models incorporated multiple stages and dual discriminators Iizuka et al. [2017], Yu et al. [2018] to ensure both local detail and global consistency. These advances enable removing an object from an image and hallucinating the covered background, providing a clean slate on which a new foreground can be inserted.

In parallel, image composition methods focus on inserting a new object into a background image in a realistic manner. This involves determining a plausible location, scale, and blending for the foreground object Lee et al. [2018], Avrahami et al. [2022], Ye et al. [2023], Creative [2024]. Traditional “copy-paste” Mortensen and Barrett [1995] often yields implausible results, so learning-based methods emerged to automate object placement and harmonization. For instance, ST-GAN (Spatial Transformer GAN) applied a learned geometric transform to warp a foreground object such that it fits naturally into the target scene Li et al. [2023b]. Later approaches used conditional GANs and transformers to model semantic context: given a background (or its segmentation map), they predict where an object of a certain class could be placed and even generate its shape if needed. These models learn common-sense placement by analyzing the background context. Beyond placement, the composite must be visually seamless. Research on image harmonization and blending addresses color and illumination matching, as well as boundary smoothing and shadow generation for inserted objects. Incorporating these aspects, multitask frameworks have been proposed to produce realistic results Dong et al. [2024].

A.2 Image Editing

A broad class of image editing methods allows modifying an image’s content while keeping other aspects unchanged. Early conditional generative models demonstrated this capability on constrained domains: for instance, facial attribute editing GANs could add or remove features like glasses or hair color “by only changing what you want” and leaving all other facial details intact Xu et al. [2018]. Another line of work uses direct image-to-image diffusion or transformer models conditioned on editing instructions Kavar et al. [2023], Zhang et al. [2023a], Rout et al. [2024,?], Mou et al. [2024], Black Forest Labs [2025], Liu et al. [2025]. These models take an image and a high-level edit description, then produce a new image with similar background and different entity. For example, Brooks et al. [2023] is a diffusion-based editor trained on synthetic “before and after” image pairs with text instructions.

A.3 Attention Editing

Attention editing method for coupled image generation leverage the internal attention mechanisms of deep generative models to control what content is preserved or changed between images Hertz et al. [2022], Yang et al. [2023], Cao et al. [2023], Mokady et al. [2023], Kim et al. [2023], Chen et al. [2024], Phung et al. [2024], Wang et al. [2024b]. In particular, diffusion models with cross-attention (e.g. Stable Diffusion Rombach et al. [2022], Imagen) allow a fine-grained alignment between text tokens and image regions. Researchers have found that by intervening in these attention maps, one can achieve text-driven edits that lock certain parts of the image in place. For example, Hertz et al. [2022] demonstrates that simply replacing a word in the text prompt usually yields a completely different image with changed background and composition. However, by injecting the cross-attention maps from the original generation into the new diffusion process, they can replace centered object while keeping the background similar. In other words, the model is guided to reuse the layout and scene details from the first image and only alter the features tied to the changed word. This ability to perform localized prompt-based editing via attention editing is a powerful tool for generating coupled images that share background/content except for specific elements. Another notable advantage is that these methods can operate without explicit masks: the “mask” is effectively created by the attention focusing on the tokens of interest Mokady et al. [2023].

B Additional Experiments

In this section, we present additional experiments and ablation studies to compare our method to existing methods. The results further validate the effectiveness of our method in both keeping a similar background and maintaining text-image alignment for the coupled image generation task.

B.1 Additional Examples

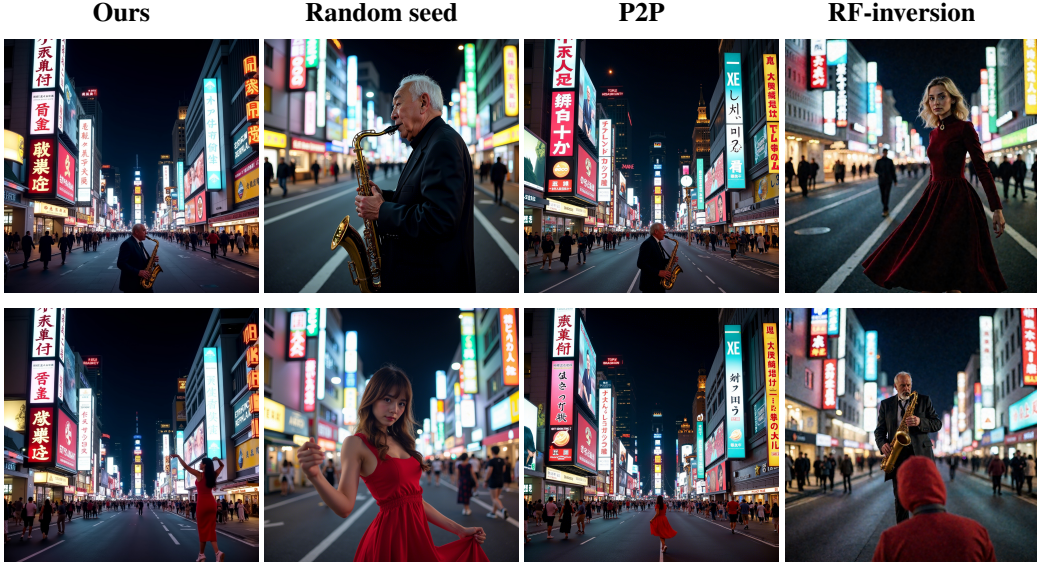


Figure 4: Comparison of our method to other baselines. Generated pictures in the first row correspond to prompt: "An elderly man in a suit playing saxophone on Tokyo night street, adorned with neon lights and billboards.". The second row corresponds to prompt: "A young woman in a red dress dancing on Tokyo night street, adorned with neon lights and billboards." Our method performs better than baselines in both background similarity and text-image alignment, where our method and all baseline methods share the same sampling procedures and random numbers.

Table 2: Metrics for coupled image generation in Figure 4

Metrics \ Model.	Ours	Random seed	P2P	RF-inversion
Background similarity ($\times 10^{-4}$) (\uparrow)	-8.663	-38.62	-11.43	-50.5
Text-image alignment (\uparrow)	17.31	16.72	15.36	11.21
Combined metric (\uparrow)	1.063	-0.3458	0.8636	-0.7018

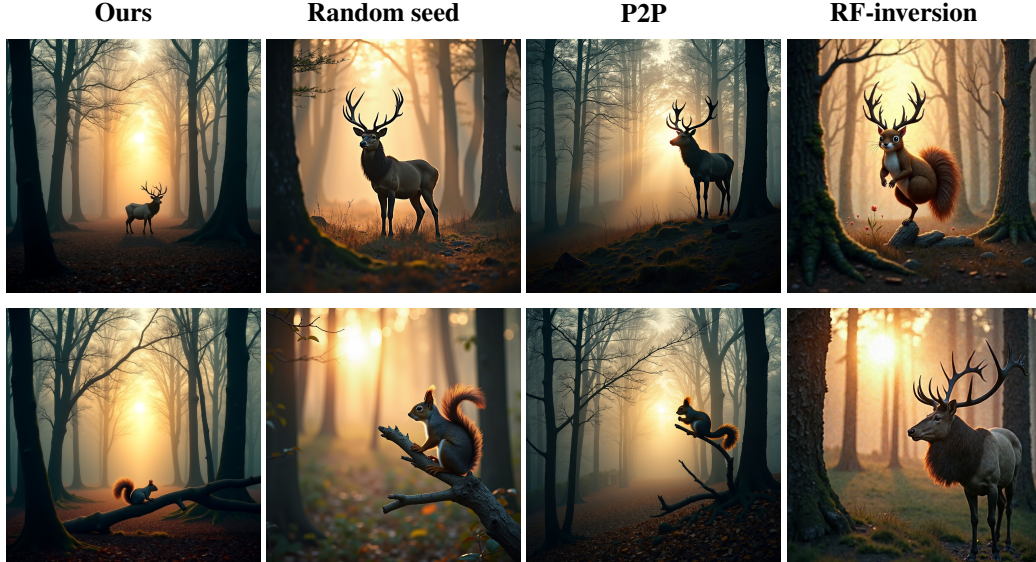


Figure 5: Comparison of our method to other baselines. Generated pictures in the first row correspond to prompt: "A majestic stag standing proud in a misty forest at dawn, sunlight through trees.". The second row corresponds to prompt: "A squirrel perched on a branch in a misty forest at dawn, sunlight through trees." Our method performs better than baselines in both background similarity and text-image alignment, where our method and all baseline methods share the same sampling procedures and random numbers.

Table 3: Metrics for coupled image generation in Figure 5

Metrics \ Model.	Ours	Random seed	P2P	RF-inversion
Background similarity ($\times 10^{-4}$) (\uparrow)	-4.953	-12.13	-5.585	-30.79
Text-image alignment (\uparrow)	21.72	20.47	19.81	16.59
Combined metric (\uparrow)	1.413	1.099	1.296	0.253

B.2 Visualization of the Time-varying Parameters

In this section, we directly visualize the time-varying parameters after solving the isotonic optimization problem, as proposed in Section 4.3. We observe that these time-varying parameters follow a common pattern, starting near 0 and gradually approaching 1 over time. This aligns with the previous findings in Choi et al. [2022], Park et al. [2023], Yue et al. [2024], Wang et al. [2024a] that diffusion models initially focus on generating coarse structure and subsequently refining fine-grained details. Indeed, the time-varying parameters are close to 0 at the initial stage of inference to ensure the generated images share a similar background. As timestep increases, the time-varying parameters also increase and approximate 1 to refine the entity features and maintain text-image alignment.

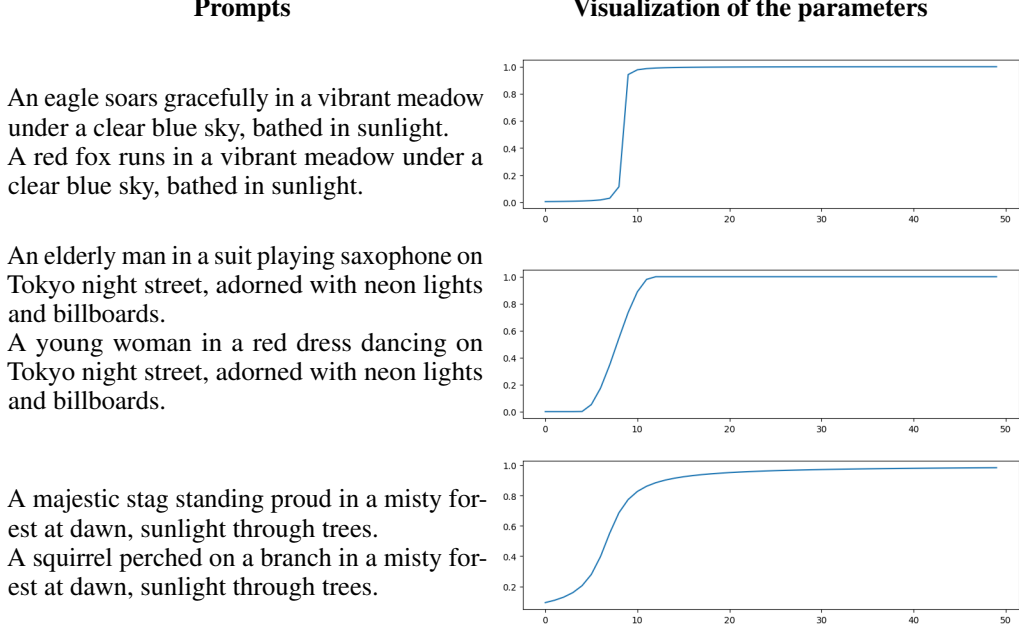


Figure 6: Visualization of the trained time-varying parameters used in the three examples.

B.3 Ablation Studies

B.3.1 Ablation Studies on Parameterized Functions

To further simplify the training load for optimizing the time-varying parameters, we propose to use three classes of parameterized functions to substitute the time-varying parameters. These functions reduce the computational efforts by restricting the number of independent variables.

- **"01" Function:** This function defines θ as a binary value. To the left of the 'center' point, θ is 0, and to the right of the 'center' point, θ is 1. Mathematically, if t is the time variable and c is the 'center' point:

$$\theta(t) = \begin{cases} 0 & \text{if } t < c \\ 1 & \text{if } t \geq c \end{cases}$$

- **"arctan" Function:** This function utilizes a transformed arctangent curve. The standard $\arctan(x)$ function is scaled and shifted such that its output is 0.5 at the 'center' point c . A common transformation to achieve $\theta(c) = 0.5$ and scale the output to approximately $[0, 1]$ could be:

$$\theta(t) = \frac{1}{\pi} \arctan(k(t - c)) + 0.5$$

where k is a scaling factor controlling the steepness of the transition.

- **"sin" Function:** This function uses a transformed sine wave. The sine function is shifted so that its value is 0.5 at the 'center' point c . Furthermore, the function is clamped: for input values that would map to an angle of $-\pi/2$ or less in the sine function's argument (after transformation), θ is set to 0. For input values that would map to an angle of $\pi/2$ or more, θ is set to 1. This effectively uses a portion of the sine wave to transition from 0 to 1. The function can be defined as:

$$\theta(t) = \begin{cases} 0 & \text{if } t \leq t_{-\pi/2} \\ \frac{1}{2} \sin(k(t - c)) + 0.5 & \text{if } t_{-\pi/2} < t < t_{\pi/2} \\ 1 & \text{if } t \geq t_{\pi/2} \end{cases}$$

Here, c is the 'center' where $k(t - c) = 0$, resulting in $\theta(c) = \frac{1}{2} \sin(0) + 0.5 = 0.5$. The points $t_{-\pi/2}$ and $t_{\pi/2}$ are defined such that $k(t_{-\pi/2} - c) = -\pi/2$ (where θ transitions to

0) and $k(t_{\pi/2} - c) = \pi/2$ (where θ transitions to 1). The parameter k controls the width of the transition.



Figure 7: Comparison of different parameterized functions. The prompts are "A majestic stag standing proud in a misty forest at dawn, sunlight through trees." and "A squirrel perched on a branch in a misty forest at dawn, sunlight through trees."

Table 4: Metrics for coupled image generation in Figure 7

Metrics \ Model.	01	arctan	sin
Background similarity ($\times 10^{-4}$) (\uparrow)	-4.55	-4.953	-4.263
Text-image alignment (\uparrow)	19.05	21.72	22.22
Combined metric (\uparrow)	1.293	1.413	1.462

The results indicate that the arctan and sin functions slightly outperform the binary 0-1 function. We attribute this improvement to the inherent smoothness of the arctan and sin functions. Unlike the 0-1 function, which introduces abrupt transitions, the gradual transitions provided by arctan and sin functions offer greater flexibility and smoother progression from 0 to 1.

B.3.2 Ablation Studies on Center and Scale of the Parameterized Functions

In this ablation study, we compare the effects of varying the center of the parameterized functions. The prompts we used are "A majestic stag standing proud in a misty forest at dawn, sunlight through trees." and "A squirrel perched on a branch in a misty forest at dawn, sunlight through trees.". The generated results are shown in Figures 8, 9, and 10.

We observe a clear trade-off between background similarity and text-image alignment. When the center value is small, fewer parameters remain near 0 while more approach 1. This leads to stronger text-image alignment but reduced background similarity. Conversely, increasing the center causes more parameters to stay near 0 and fewer to approach 1, which improves background similarity at the cost of alignment with the text prompt. To navigate this trade-off, we formulate and solve the isotonic optimization problem and identify a balance that achieves both high background similarity and strong text-image alignment.

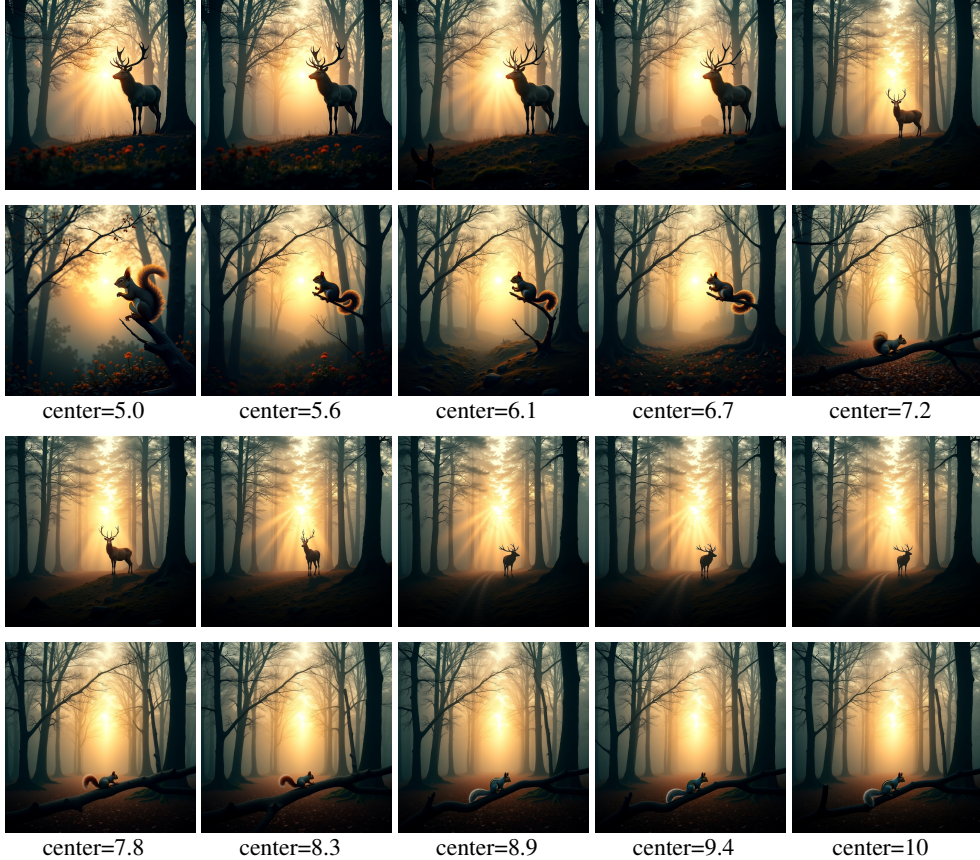


Figure 8: Comparison of different parameter centers. (sin) (scale=0.8)

C Prompt Example

We present the example of prompting a pre-trained LLM to extract the shared background and present the distinct entity descriptions in Figure 11.



Figure 9: Comparison of different parameter centers. (arctan) (scale=0.5)

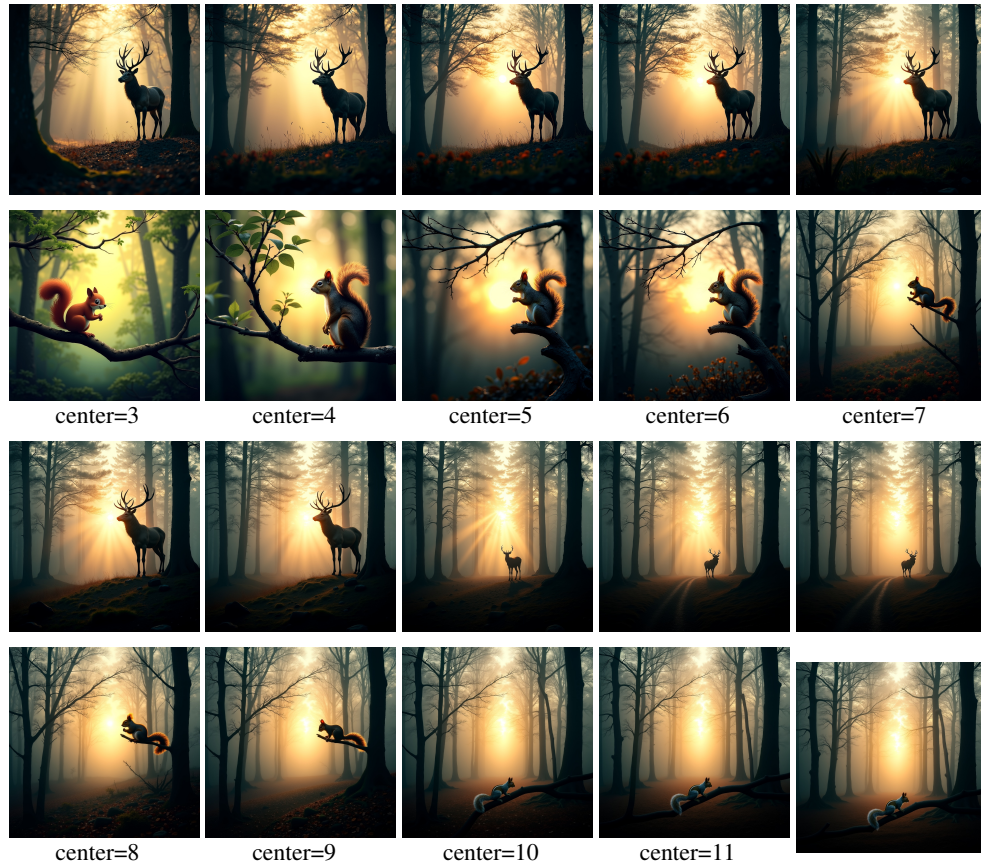


Figure 10: Comparison of different parameter centers. (01) center=12

User Input:

role: system, content: You are a helpful assistant to arrange prompts for text-to-image generation.

role: user, content: You are given a set of prompts for text-to-image generation. Your task is to first identify and extract the common background shared across all prompts. Then, for each individual prompt, present the distinct entity description. Please format your output as follows: Background: [shared background] Entity 1: [description of the first unique entity] Entity 2: [description of the second unique entity] ... and so on.

role: user, content: Prompt 1: A cute Pikachu sits in a cozy room bathed in warm sunshine. The room has wooden flooring and a peaceful, homely atmosphere. Prompt 2: A beautiful girl stands in a cozy room bathed in warm sunshine. The room has wooden flooring and a peaceful, homely atmosphere."



LLM Output:

Background: A cozy room bathed in warm sunshine with wooden flooring and a peaceful, homely atmosphere.

Entity 1: A cute Pikachu sits.

Entity 2: A beautiful girl stands.

Figure 11: A zero-shot example of prompting a pre-trained LLM to extract the shared background from a set of prompts and present the distinct entity descriptions for each individual prompt.